PAPER

New formulation for the recursive transfer method using the weak form theory framework and its application to microwave scattering

Hatsuhiro KATO[†a)], *Member and* **Hatsuyoshi KATO**[††], *Nonmember*

SUMMARY The recursive transfer method (RTM) is a numerical technique that was developed to analyze scattering phenomena and its formulation is constructed with a difference equation derived from a differential equation by Numerov's discretization method. However, the differential equation to which Numerov's method is applicable is restricted and therefore the application range of RTM is also limited. In this paper, we provide a new discretization scheme to extend RTM formulation using the weak form theory framework. The effectiveness of the proposed formulation is confirmed by microwave scattering induced by a metallic pillar placed asymmetrically in the waveguide. A notable feature of RTM is that it can extract a localized wave from scattering waves. The discrepancy between the experimental and theoretical data is suppressed with in an upper bound determined by the standing wave ratio of the waveguide.

key words: *Recursive Transfer Method, Weak Form Theory, Microwave Scattering, Localized Wave, Numerical Method*

1. Introduction

Numerov's method is a discretization method to derive a difference equation from a differential equation. It was developed to analyze a wave function of atomic orbits [1]. Using Numerov's method, the recursive transfer method (RTM) was developed to analyze the electron conductance [2], [3] and microwave scattering [4], [5]. However, the differential equations to which Numerov's method is applicable are restricted and therefore, phenomena that can be analyzed by RTM is also limited. The purpose of this paper is to propose a new discretization scheme to extend RTM formulation based on the framework of the weak form theory. As a typical example of an application of the proposed theory, a microwave scattering problem in waveguides is chosen because an accurate experiment through a reliable system can be used to validate it.

To analyze microwave scattering and absorption, various numerical methods have been proposed such as the finite element method (FEM) [7], integral equation formulation [8], [9], mode analysis of waveguides [10], impeadance matrix formulation [11], finite-difference-time-domain method, beam propagation method (BPM) and combinations of these methods [12]. If the system is periodic, the scattering matrix method is an effective numerical method [13]. In contract, if the system is non periodic, the bidirectional eigenmode propagation method [14] and fast Fourier transformation beam propagation method (FFT-BPM) [15], [16] can analyze reflection and transmission phenomena, but those require eigenmode analysis at each site along the propagation axis when the scatterer has a complex shape. However, RTM does not require eigenmode analysis at sites in the scattering region. Furthermore, the stability of the solution obtained by RTM has been well understood and confirmed [1], [17].

The RTM formulation is in some sense an improvement of the transfer matrix formulation [18], or scattering matrix theory [19]. Instead of field strengths, step-on matrices are used to express the field entity as a medium to propagate waves. A step-on matrix is also used to express the boundary conditions that is a numerically realized absorbing boundary condition (ABC) [7]. A significant feature of the proposed RTM is that it can extract a localized wave around the scatterer. This feature is already used to analyze an absorption mechanism [5]. The transfer matrix method is also able to use the wave extraction in infinite space [19], however, it is not applicable to waves in a waveguide. RTM is the first method that can extract localized waves around the scatterer in a waveguide.

In a previous paper, we applied RTM to analyze scattering and absorption processes in a waveguide [4], where the boundary condition at the inner wall was considered under an assumption that the shape of the scatterer has an inversion symmetry. Using a functional expression with Lagrangian multipliers and according to the weak form theory framework, this restriction on the scatterer shape is removed.

The paper is organized as follows. In section 2, the difference equation for microwave scattering is derived on the basis of the weak form theory framework. The boundary condition at the inner wall of the waveguide is incorporated into the coefficients of the difference equation. Associated with functional formulation, an important parameter θ is introduced, which affects the analyzing accuracy of RTM. In section 3, the RTM procedure used to solve the derived difference equation is summarized. An appropriate value for the parameter θ is determined in this section with respect to the accuracy of the plane wave expressions. In section 4, a scattering experiment is used to confirm the effectiveness of the proposed theory. The last section is devoted to the conclusion and two addional features of RTM are discussed in the appendices.

Manuscript received April **, 2012.

[†]The author is with the Interdisciplinary Graduate School of Medicine and Engineering, University of Yamanashi, Takeda, 4-3-11, Kofu, Yamanashi, 400-8511 Japan.

[††]The author is with the Tomakomai National College of Technology, 433, Nishikioka, Tomakomai, Hokkaido, 059-1275, Japan.

a) E-mail: katoh@yamanashi.ac.jp

DOI: 10.1587/trans.E0.??.1

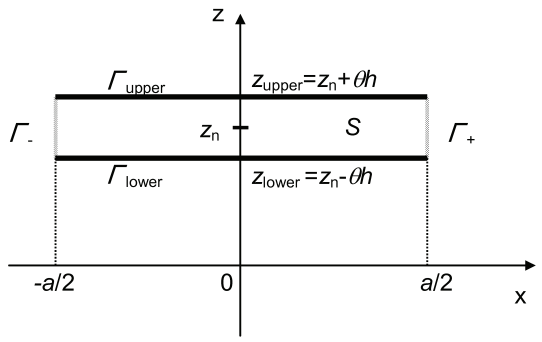

Fig. 1 Integration region of the functional.

2. Weak form scheme to derive the difference equation

2.1 Functional for the scattering problem

Let us consider a two-dimensional system where a field variable $u(z, x)$ is subjected to a second-order differential equation as follows,

$$\frac{\partial^2 u}{\partial z^2} + \frac{\partial^2 u}{\partial x^2} + v(z, x)u = 0. \tag{1}$$

This is a generalized form of the Helmholtz equation that is valid in many systems. In the case of microwaves, the function $u(z, x)$ can be regarded as an electric field polarized along the y-axis. When the scatterer is composed of a dissipative material, the function $v(z, x)$ takes complex values [4], [5]. The following formulation will be constructed for microwaves in a waveguide, but it is possible to apply it to any system subject to (1).

In Fig. 1, an imaginary extracted part of a rectangular waveguide is shown. The wave guide is assumed to be of a uniform width a in the x-axis direction. The lower and upper limits of the extracted wave guide are located at $z = z_{\text{lower}}$ and $z = z_{\text{upper}}$, respectively, $S = [z_{\text{lower}}, z_{\text{upper}}] \times [-a/2, a/2]$. The field $u(z, x)$ is assumed to vanish at the inner walls of the waveguide, $\Gamma_{\pm} = [z_{\text{lower}}, z_{\text{upper}}] \times \{\pm a/2\}$. Considering the boundary condition as a constraint on the field and introducing operators R_ρ ($\rho = \pm$) defined by $R_\rho(u) = u(z, \rho a/2)$, the boundary condition on the field is expressed as follows,

$$R_\rho(u) = 0, \quad (z, x) \in \Gamma_\rho. \tag{2}$$

Though several procedures can be used to obtain a weak form functional through which a solution of the differential equation (1) can be obtained, a successful candidate is derived from the following functional,

$$F[u] = \frac{1}{2}\int_S \left[-(\nabla u)^2 + v(z, x)u^2\right] dS - \sum_{\rho=\pm}\int_{\Gamma_\rho} R_\rho(u)\lambda_\rho d\ell, \tag{3}$$

where ∇ is defined by $\nabla = [\partial/\partial z, \partial/\partial x]^T$ and dS and $d\ell$ are the infinitesimal area and line element, respectively. The parameter $\lambda_\rho(z, x)$ is a Lagrangian multiplier, which alters condition (2) and makes the field $u(z, x)$ unrestricted. Using a parameter ϵ and an arbitrary field $w(z, x)$, a new functional $F'[w, u]$ is introduced following a concept of the Gateaux derivative [20] as follows,

$$F'[w, u] = \lim_{\epsilon\to 0}\frac{1}{\epsilon}(F[u + \epsilon w] - F[u]), \tag{4}$$

which is identical to the first variation of the functional $F[u]$ [21], [22]. The functional $F'[w, u]$ can be expressed in an integral form as follows,

$$F' = \int_S [-\nabla w \cdot \nabla u + wv(z, x)u]\, dS - \sum_{\rho=\pm}\int_{\Gamma_\rho} R'_\rho(w, u) d\ell. \tag{5}$$

Here, the operator $R'_\rho(w, u)$ is defined as follows,

$$R'_\rho(w, u) = \lim_{\epsilon\to 0}\frac{1}{\epsilon}\Big[R_\rho(u + \epsilon w) - R_\rho(u)\Big]. \tag{6}$$

Because the operator $R_\rho(u)$ is linear with respect to $u(z, x)$, the operator $R'_\rho(w, u)$ is independent of the function $u(z, x)$ and $R'_\rho(w, u) = w(z, \rho a/2)$. The ability of the functional (5) to serve as an alternative to the differential equation (1) can be confirmed as follows.

Using the identity relation $\nabla w \cdot \nabla u = -w\nabla^2 u + \nabla \cdot (w\nabla u)$ and Gauss' theorem, the functional F' can be transformed into

$$F' = \int_S w\left[\frac{\partial^2 u}{\partial z^2} + \frac{\partial^2 u}{\partial x^2} + v(z, x)u\right] dS - \sum_{\rho=\pm}\int_{\Gamma_\rho}\left[w\frac{\partial u}{\partial n} + R'_\rho(w, u)\lambda_\rho\right] d\ell. \tag{7}$$

Here, $\partial u/\partial n$ is the directional derivative from the boundary Γ_ρ to the external side of the region S. Further, to eliminate the linear integrals in (7) at the lower boundary Γ_{lower}($= \{z_{\text{lower}}\} \times [-a/2, a/2]$) and the upper boundary Γ_{upper} ($= \{z_{\text{upper}}\} \times [-a/2, a/2]$), the following condition is assumed,

$$w(z, x) = 0, \quad (z, x) \in \Gamma_{\text{lower}}, \Gamma_{\text{upper}}. \tag{8}$$

Because of this condition, no natural boundary condition is imposed on Γ_{lower} and Γ_{upper} associated with the null value problem of the functional (5). Here, the null value problem is stated as "what is the function $u(z, x)$ that satisfies $F'[w, u] = 0$ for the arbitrary function $w(z, x)$?".

The surface integral over the region S in (7) implies that the field variable $u(z, x)$ is a solution of the differential equation (1), when it satisfies the null value condition $F'[w, u] = 0$ for arbitrary $w(z, x)$. Although the functional expressions (5) and (7) are transformed mutually, the condition imposed on the field $u(z, x)$ depends on which of the two expressions is used. When the form (7) is used, the variable $u(z, x)$ must be differentiable twice. On the other hand, if the

expression (5) is used, the field $u(z, x)$ is sufficient to be differentiable only once. Therefore, the requirement for $u(z, x)$ is weakened and the solution for the null value problem of the functional (5) can be termed a weak solution [6].

Because of the linear integrations on Γ_ρ in (7), the Lagrangian multipliers $\lambda_\rho(x)$ affect the boundary values of $\frac{\partial}{\partial n}u$. Using the freedom to choose the multipliers and adjusting the value of $\frac{\partial}{\partial n}u$, one can satisfy the constraint conditions (2).

2.2 Discretization of the fields with respect to the x-axis

For the numerical calculation, the interval $[-a/2, a/2]$ on the x-axis is divided into N_x parts and the coordinates are discretized as follows,

$$x_\ell = x_0 + h_x \cdot \ell, \tag{9}$$

where the initial value $x_0 = -a/2$, the step size $h_x = a/N_x$, and the index $\ell = 0, 1, 2, ..., N_x$. The fields $u(z, x)$, $w(z, x)$, and $v(z, x)$ are also digitized with respect to the variable x and expanded, respectively, in a finite series as follows,

$$u(z, x_\ell) = \sum_p \varphi_p(z) e^{i(k_x+G_p)x_\ell}, \tag{10}$$

$$w(z, x_\ell) = \sum_p \psi_p(z) e^{-i(k_x+G_p)x_\ell}, \tag{11}$$

and

$$v(z, x_\ell) = \sum_p v_p(z) e^{iG_p x_\ell}. \tag{12}$$

The wave number G_p is defined by $G_p = 2\pi p/a$ with the index $p = -[N_x/2], ..., -1, 0, 1, ..., [(N_x - 1)/2]$, where the notation $[r]$ represents the maximum integer that does not exceed the real number r. The parameter k_x is an arbitrary constant, whose value is selected to achieve efficient expansions. We select the value k_x as $k_x = \pi/a$, which realizes an exact expansion for the incident wave in the TE_{10} mode [4]. A consideration for the influence of the arbitrary parameter k_x is given in Appendix A. The value of the field at an arbitrary site x, that is not always on one of the discretized points x_ℓ, is interpolated by the series expansions given in (10), (11), and (12).

The field vector $\mathbf{\Phi}(z)$ is defined as a column vector that is composed of the expansion coefficients $\varphi_p(z)$ in (10) so that $\mathbf{\Phi}(z) = [..., \varphi_{-1}(z), \varphi_0(z), \varphi_1(z), ...]^T$. Hereafter, the shortened expression $\mathbf{\Phi}(z) = \{\varphi_p(z)\}$ is used, where the index p in the brackets takes whole values of the index range. In the same manner, the field vector $\mathbf{\Psi}(z)$ is defined by $\mathbf{\Psi}(z) = \{\psi_p(z)\}$ and the vector $\mathbf{d}(x)$ is defined by $\mathbf{d}(x) = \{e^{i(k_x+G_p)x}\}$. Now, the fields $u(z, x)$ and $w(z, x)$ can be expressed as $u(z, x) = \mathbf{d}(x)^T\mathbf{\Phi}(z)$ and $w(z, x) = \mathbf{d}(x)^{*T}\mathbf{\Psi}(z)$, respectively, where $\mathbf{d}(x)^* = \{e^{-i(k_x+G_p)x}\}$. Because $\mathbf{d}(\pm a/2) = e^{\pm ik_x a/2}\mathbf{d}_0$ with $\mathbf{d}_0 = \{(-1)^p\}$, the two constraint conditions (2) are reduced to one condition as follows,

$$\mathbf{d}_0^T\mathbf{\Phi}(z) = 0. \tag{13}$$

Then, the constraint term in the functional (5) can also be expressed in a reduced form as follows,

$$\sum_{\rho=\pm} R'_\rho(w, u)\lambda_\rho = \mathbf{\Psi}(z) \cdot \mathbf{d}_0\lambda(z). \tag{14}$$

where $\lambda(z)$ is a degenerate function of the multipliers defined as $\lambda(z) = e^{-ik_x a/2}\lambda_+(z) + e^{ik_x a/2}\lambda_-(z)$.

Substituting the series expansions (10), (11), and (12) for the corresponding expressions in (5) yield the following matrix form,

$$F' = a\int_{z_{\text{lower}}}^{z_{\text{out}}} \left[-\frac{d\mathbf{\Psi}}{dz} \cdot \frac{d\mathbf{\Phi}}{dz} + \mathbf{\Psi} \cdot \bar{V}(z)\mathbf{\Phi}\right] dz - \int_{z_{\text{lower}}}^{z_{\text{out}}} \mathbf{\Psi} \cdot \mathbf{d}_0\lambda(z)dz. \tag{15}$$

Here, $\bar{V}(z)$ is a matrix defined by

$$\bar{V}(z) = [-(k_x + G_p)^2\delta_{p,q} + v_{p-q}(z)], \tag{16}$$

where $\delta_{p,q}$ is the Kronecker delta. Hereafter, the notation with super bar, $\bar{}$, indicates a matrix of size $N_x \times N_x$. This expression of the functional plays an important role in deriving the difference equation in the next section.

2.3 Discretization of the fields with respect to the z-axis

The z-axis is set along the direction in which the wave propagates and the incident wave originates from the terminal $z = z_{\text{in}}$. The scatterer is assumed to be included in the region $z_{\text{in}} < z < z_{\text{out}}$, where the coordinates z_{in} and z_{out} are the lower and the upper bounds of the analyzing region, respectively. The analyzing region is divided into N_z parts and discretized as follows,

$$z_n = z_0 + h_z \cdot n, \tag{17}$$

where the initial value is $z_0 = z_{\text{in}}$, the step width is defined by $h_z = (z_{\text{out}} - z_{\text{in}})/N_z$ and the index $n = 0, 1, 2, ..., N_z$. Then, the upper terminal of the system is given by $z_{N_z} (= z_{\text{out}})$.

In the functional expression (15), the integral region $[z_{\text{lower}}, z_{\text{upper}}]$ can be chosen according to the solution procedures. In the case of FEM, the integral region is chosen so as to include the whole scatterer in the integral region. In the case of RTM, the integral region is selected as a narrow region around a discretized site z_n and the functional is regarded as a local entity. The role of the local functional is to obtain the difference equation of the discretized field $\mathbf{\Phi}(z)$. Therefore, the integration regions in the functional F' are defined as $z_{\text{lower}} = z_n - \theta h_z$, $z_{\text{upper}} = z_n + \theta h_z$, where θ is an important parameter, whose value is chosen so as to achieve high accuracy (see section 3.3).

Using the quadratic interpolation functions $L_n^{(0)}(z)$ and $L_n^{(\pm 1)}(z)$ defined by

$$L_n^{(+1)}(z) = \frac{1}{2h_z^2}(z - z_n)(z - z_{n-1}), \tag{18}$$

$$L_n^{(0)}(z) = \frac{-1}{h_z^2}(z - z_{n+1})(z - z_{n-1}), \tag{19}$$

$$L_n^{(-1)}(z) = \frac{1}{2h_z^2}(z - z_{n+1})(z - z_n), \tag{20}$$

the field vectors $\mathbf{\Phi}(z)$ and $\mathbf{\Psi}(z)$ and the multiplier $\lambda(z)$ are interpolated in the region $z_{n-1} < z < z_{n+1}$ with three terms at z_{n+p} $(p = 0, \pm 1)$ as follows,

$$\mathbf{\Phi}(z) = \sum_{p=0,\pm1} \mathbf{\Phi}(z_{n+p}) L_n^{(p)}(z), \tag{21}$$

$$\mathbf{\Psi}(z) = \sum_{p=0,\pm1} \mathbf{\Psi}(z_{n+p}) L_n^{(p)}(z), \tag{22}$$

$$\lambda(z) = \sum_{p=0,\pm1} \lambda(z_{n+p}) L_n^{(p)}(z). \tag{23}$$

The constraint condition (8) for the arbitrary field $u(z, x)$ imposes a constraint such that

$$\mathbf{\Psi}(z_{n+1}) = \mathbf{\Psi}(z_{n-1}) = (1 - 1/\theta^2)\mathbf{\Psi}(z_n). \tag{24}$$

In the expression (22), three terms of $\mathbf{\Psi}(z_{n+p})$ $(p = 0, \pm 1)$ appear but only $\mathbf{\Psi}(z_n)$ is an independent term.

2.4 Derivation of the difference equation

Using the interpolated expressions (21), (22), and (23), and the condition (24), all the integrals in the form (5) can be performed and the functional $F'[w, u]$ is transformed into an discretized expression with $\mathbf{\Phi}(z_{n+p})$, $\lambda(z_{n+p})$ $(p = 0, \pm 1)$ and $\mathbf{\Psi}(z_n)$. The transformation is realized through lengthy but straightforward calculations and one finds that the expression of F' has a multiplication form between $\mathbf{\Psi}(z_n)$ and the linear combination of $\mathbf{\Phi}(z_{n+p})$ and $\lambda(z_{n+p})$. Because $\mathbf{\Psi}(z_n)$ is arbitrary, the null value problem of F' leads to a second-order difference equation for $\mathbf{\Phi}(z_{n+p})$ and $\lambda(z_{n+p})$, which is expressed as follows,

$$\begin{aligned} &\bar{a}_n\mathbf{\Phi}(z_{n+1}) + \bar{b}_n\mathbf{\Phi}(z_n) + \bar{c}_n\mathbf{\Phi}(z_{n-1}) \\ &-\frac{1}{a}\mathbf{d}_0\Big[\alpha\lambda(z_{n+1}) + 2\beta\lambda(z_n) + \alpha\lambda(z_{n-1})\Big] = 0. \end{aligned} \tag{25}$$

Here, the constants α and β are defined by

$$\alpha = \frac{\theta^2}{10}, \quad \beta = \frac{5 - \theta^2}{10}, \tag{26}$$

and the coefficient matrices $\bar{a}_n$, $\bar{b}_n$ and $\bar{c}_n$ are given by

$$\bar{a}_n = \bar{I} + \alpha h_z^2 \bar{V}(z_{n+1}), \tag{27}$$

$$\bar{b}_n = -2\bar{I} + 2\beta h_z^2 \bar{V}(z_n), \tag{28}$$

$$\bar{c}_n = \bar{I} + \alpha h_z^2 \bar{V}(z_{n-1}), \tag{29}$$

where $\bar{I}$ is the identity matrix whose size is equal to that of the matrix $\bar{V}(z)$.

Multiplying the both sides of (25) by the term $\mathbf{d}_0^T$ from the left and using the constraint condition (13), we obtain the following condition,

$$\begin{aligned} &\alpha\ [h_z^2\mathbf{d}_0^T\bar{V}(z_{n+1})\mathbf{\Phi}(z_{n+1}) - \frac{N_x}{a}\lambda(z_{n+1})] \\ &+\ 2\beta[h_z^2\mathbf{d}_0^T\bar{V}(z_n)\mathbf{\Phi}(z_n) - \frac{N_x}{a}\lambda(z_n)] \\ &+\ \alpha[h_z^2\mathbf{d}_0^T\bar{V}(z_{n-1})\mathbf{\Phi}(z_{n-1}) - \frac{N_x}{a}\lambda(z_{n-1})] = 0. \end{aligned} \tag{30}$$

Here, the relation $\mathbf{d}_0^T\mathbf{d}_0 = N_x$ has been used. The solution of (30) is found as

$$\lambda(z_n) = \frac{ah_z^2}{N_x}\mathbf{d}_0^T\bar{V}(z_n)\mathbf{\Phi}(z_n). \tag{31}$$

If another multiplier $\lambda'(z_n)$ exists as a solution of (30) for the same field vector $\mathbf{\Phi}(z_n)$, one can derive from (25) that the difference $\Delta(z_n) = \lambda'(z_n) - \lambda(z_n)$ satisfies the following equation

$$\alpha\Delta(z_{n+1}) + 2\beta\Delta(z_n) + \alpha\Delta(z_{n-1}) = 0. \tag{32}$$

The solution of this equation is easily obtained as $\Delta(z_n) \propto (-\beta \pm \sqrt{\beta^2 - \alpha^2})^n$. Although the multiplier defined by (31) is found heuristically, the solution is unique except for the arbitrariness of $\Delta(z_n)$. Further, the function $\lambda(z_n)$ is unique in the sense of a weak solution [6].

Substituting the relation (31) for terms in the difference equation (25) yields

$$\bar{a}'_n\mathbf{\Phi}(z_{n+1}) + \bar{b}'_n\mathbf{\Phi}(z_n) + \bar{c}'_n\mathbf{\Phi}(z_{n-1}) = 0. \tag{33}$$

Here, the coefficient matrices are given by

$$\bar{a}'_n = \bar{I} + \alpha\Big(\bar{I} - \frac{\mathbf{d}_0\mathbf{d}_0^T}{N_x}\Big)h_z^2\bar{V}(z_{n+1}), \tag{34}$$

$$\bar{b}'_n = -2\bar{I} + 2\beta\Big(\bar{I} - \frac{\mathbf{d}_0\mathbf{d}_0^T}{N_x}\Big)h_z^2\bar{V}(z_n), \tag{35}$$

$$\bar{c}'_n = \bar{I} + \alpha\Big(\bar{I} - \frac{\mathbf{d}_0\mathbf{d}_0^T}{N_x}\Big)h_z^2\bar{V}(z_{n-1}). \tag{36}$$

Considering the boundary condition of the inner walls of the waveguide as a constraint condition, the partial differential equation (1) was transformed into the second-order difference equation (33). A significant feature of the equation (33) appears in the coefficients that include terms related to the boundary condition.

3. RTM formulation

3.1 Step-on matrices and their scattering free expressions

RTM is a method that uses step-on matrices as the field variables instead of the field vectors $\mathbf{\Phi}(z_n)$. The step-on matrix $\bar{S}_n$ is defined by

$$\mathbf{\Phi}(z_{n+1}) = \bar{S}_n\mathbf{\Phi}(z_n), \tag{37}$$

and the recurrence relation about $\bar{S}_n$ is derived from (33) as follows [2],

$$\bar{S}_{n-1} = -(\bar{a}'_n\bar{S}_n + \bar{b}'_n)^{-1}\bar{c}'_n. \tag{38}$$

Outside the scattering region, waves propagate freely and the step-on matrix does not depend on the sites z_n. We will now define a numerical procedure to find the step-on matrices in a uniform waveguide.

In uniform waveguides, the function $v(z, x)$ is given by $v(z, x) = \omega^2\mu_0\epsilon_0$. and the matrix $\bar{V}(z_n)$ is independent of the coordinate z_n. Therefore, the index n in the relation (38) degenerates and the matrices are reduced such that $\bar{S}_n = \bar{S}_{n-1} = \bar{K}_{\rm fw}$, $\bar{a}'_n = \bar{c}'_n = \bar{a}'_0$ and $\bar{b}'_n = \bar{b}'_0$ with the constant matrices $\bar{K}_{\rm fw}$, $\bar{a}'_0$ and $\bar{b}'_0$. If a matrix $\bar{H}$ is defined to satisfy the relation

$$\cosh\bar{H} = \frac{1}{2}\bar{a}'^{-1}_0\bar{b}'_0, \tag{39}$$

the relation (38) is required to satisfy the following equation,

$$\bar{K}^2_{\rm fw} + (2\cosh\bar{H})\bar{K}_{\rm fw} + \bar{I} = 0, \tag{40}$$

for the step-on matrix $\bar{K}_{\rm fw}$. When the eigenvalues and modal matrix of $\bar{H}$ are denoted with $\eta_p h_z$ and $\bar{T}$ (p = 1, 2, ..., N_x) (*i.e.*, $\bar{H} = \bar{T}[\eta_p h_z \delta_{p,q}]\bar{T}^{-1}$), the matrix $\bar{K}_{\rm fw}$ is expressed as $\bar{K}_{\rm fw} = \bar{T}\left[e^{\eta_p h_z}\delta_{p,q}\right]\bar{T}^{-1}$. Here, the parameter η_p is the propagation constant labeled with mode number p. The real and imaginary parts of η_p are the damping/growing constant and the wave number, respectively. The system is symmetric under the z-axis inversion and time reversal transformations. Therefore, if η_p is a propagation constant, the associating four values of $\pm\eta_p$ and $\pm\eta^*$ are also the propagation constants, where the asterisk, *, indicates the complex conjugate. It is easy to show that the inverse matrix $\bar{K}^{-1}_{\rm fw}$ is also a solution of (40).

The mode with the pure imaginary propagation constant, or Re[η_p] = 0, corresponds to the traveling wave, whose traveling direction is determined by the sign of Im[η_p]. If the wave number is Im[η_p] > 0 (Im[η_p] < 0), it travels along the positive (negative) direction of the z-axis. On the other hand, if Re[η_p] < 0 (Re[η_p] > 0), the wave amplitude will dampen (grow) when the wave proceeds toward the positive direction along the z-axis. This feature is observed in localized waves that are generated in the scattering region and propagate to the adjacent region.

Using the freedom of the double sign in $\pm\eta_p$ and $\pm\eta^*_p$, the combination of propagation constants relating to the step-on matrix $\bar{K}_{\rm fw}$ can be set as follows: the amplitude will grow, Re[η_p] > 0, for the localized mode and the traveling wave will proceed toward the positive direction, Im[η_p] > 0. The notation $\bar{K}^{(\rm grw)}_+$ stands for this step-on matrix. In the same manner, other choices of sign combinations are possible and one can make four step-on matrices for $\bar{K}^{(\sigma)}_s$. Here, s(= +, −) indicates the direction of the traveling waves, and σ(= dmp, grw) stands for the damping/growing of the localized waves.

3.2 Scattering problem in RTM

The uniform wave guides are assumed to continue beyond the simulation terminals, $z \le z_0(= z_{\rm in})$ and $z \ge z_{N_z}(= z_{\rm out})$. To indicate the position beyond the terminals, the index n is allowed to take negative values and any values greater than N_z. In the input region, the wave is composed by superposing the incident and reflected waves. On the other hand, in the output region, only the transmitted wave exists. Therefore, the wave $\mathbf{\Phi}(z_n)$ is expressed as follows,

$$\mathbf{\Phi}(z_n) = \begin{cases} (\bar{K}^{(\rm grw)}_+)^n\mathbf{\Phi}_{\rm in} + (\bar{K}^{(\rm grw)}_-)^n\mathbf{\Phi}_{\rm rf}, & (n \le 1) \\ (\bar{K}^{(\rm dmp)}_+)^{(n-N_z)}\mathbf{\Phi}_{\rm tr}, & (n \ge N_z) \end{cases}, \tag{41}$$

where the field vectors of the incident, reflected, and transmitted waves are denoted as $\mathbf{\Phi}_{\rm in}$, $\mathbf{\Phi}_{\rm rf}$ and $\mathbf{\Phi}_{\rm tr}$, respectively. The notation (dmp) or (grw) is selected to satisfy the condition that the localized wave vanishes at the site far from the scatterer ($z_n \to \pm\infty$). The double sign ± or the traveling direction is selected as negative (-) for the reflected wave and positive (+) for the incident and transmitted waves.

The boundary condition under which only the transmitted wave exists at the terminal $n = N_z$, or $z = z_{N_z}$, is expressed by the step-on matrix $\bar{S}_n$ as follows,

$$\bar{S}_{N_z} = \bar{K}^{(\rm dmp)}_+. \tag{42}$$

This condition is a type of ABC [7] that reflects the following two situations: (i) Any traveling wave passes the boundary without reflection. (ii) Even if tails of localized wave reach the boundary, these propagate beyond the boundary as if the uniform waveguide continues.

Using the boundary condition (42) and the recurrence relation (38), all the step-on matrices $\bar{S}_n (n < N_z)$ can be obtained recursively. The expression $\mathbf{\Phi}(z_1) = \bar{S}_0\mathbf{\Phi}(z_0)$ is equivalent to the form $\bar{K}^{(\rm grw)}_+\mathbf{\Phi}_{\rm in} + \bar{K}^{(\rm grw)}_-\mathbf{\Phi}_{\rm rf} = \bar{S}_0(\mathbf{\Phi}_{\rm in} + \mathbf{\Phi}_{\rm rf})$. Therefore, the field vector of the reflected wave, $\mathbf{\Phi}_{\rm rf}$, can be linked to the field vector of the incident wave, $\mathbf{\Phi}_{\rm in}$, as follows,

$$\mathbf{\Phi}_{\rm rf} = -(\bar{S}_0 - \bar{K}^{(\rm grw)}_-)^{-1}(\bar{S}_0 - \bar{K}^{(\rm grw)}_+)\mathbf{\Phi}_{\rm in}. \tag{43}$$

The reason that the input region in (41) is not given by $z < z_0$ but by $z < z_1$ is to derive this expression. Using the field vector at the incident terminal $z = z_0$, $\mathbf{\Phi}(z_0) = \mathbf{\Phi}_{\rm in} + \mathbf{\Phi}_{\rm rf}$, the field vector at the n-th site ($n > 0$) is expressed as follows,

$$\mathbf{\Phi}(z_n) = \bar{S}_{n-1}\cdots\bar{S}_2\bar{S}_1\bar{S}_0\mathbf{\Phi}(z_0). \tag{44}$$

Because $\mathbf{\Phi}_{\rm tr} = \mathbf{\Phi}(z_{N_z})$, the transmitted wave is obtained by

$$\mathbf{\Phi}_{\rm tr} = \bar{S}_{N_z-1}\cdots\bar{S}_2\bar{S}_1\bar{S}_0(\mathbf{\Phi}_{\rm in} + \mathbf{\Phi}_{\rm rf}). \tag{45}$$

Thus, we have expressed the field vectors of the reflected and transmitted waves with relation to the field vector of the incident wave, $\mathbf{\Phi}_{\rm in}$.

3.3 Determination of the θ value

In unlimited free space where no scatterer and no influence from the boundary exist, the value of the parameter θ shown in Fig. 1 can be determined through the comparison of analytical solutions of the continuum and the discrete systems. In this section, the value of the parameter θ is determined.

In unlimited free space, the matrix $\bar{V}(z_n)$ is diagonal and independent of the location coordinate z_n or the index n. More specifically, the matrix $\bar{V}(z_n)$ is expressed as $\bar{V}(z_n)$ =

$[k_p^2\delta_{p,q}]$ where the parameter k_p is defined by

$$k_p = \sqrt{\omega^2\mu_0\epsilon_0 - (k_x + G_p)^2}. \tag{46}$$

Because the coefficient matrices $\bar{a}_n$, $\bar{b}_n$ and $\bar{c}_n$ are also independent of the index n, the difference equation (33) is reduced to the following diagonal form,

$$\bar{a}_0\mathbf{\Phi}(z_{n+1}) + \bar{b}_0\mathbf{\Phi}(z_n) + \bar{a}_0\mathbf{\Phi}(z_{n-1}) = 0, \tag{47}$$

$$\bar{a}_0 = \bar{I} + \alpha h_z^2[k_p^2\delta_{p,q}], \tag{48}$$

$$\bar{b}_0 = -2\bar{I} + 2\beta h_z^2[k_p^2\delta_{p,q}], \tag{49}$$

where the boundary terms have been removed. Analytic solutions of this equation, $\mathbf{\Phi}_{\pm}(z_n)$, can be easily obtained as follows,

$$\mathbf{\Phi}_{\pm}(z_n) = \bar{K}_{\pm}^n\mathbf{\Phi}_{0\pm}, \tag{50}$$

where $\mathbf{\Phi}_{0\pm}$ is an arbitrary constant vector and the matrices $\bar{K}_{\pm}$ are defined by

$$\bar{K}_{\pm} = \left[e_p^{(\pm)}\delta_{p,q}\right], \tag{51}$$

$$e_p^{(\pm)} = \left(\frac{1-\beta h_z^2k_p^2}{1+\alpha h_z^2k_p^2}\right) \pm \sqrt{\left(\frac{1-\beta h_z^2k_p^2}{1+\alpha h_z^2k_p^2}\right)^2 - 1}. \tag{52}$$

The step-on matrix $\bar{K}_{\rm fw}$ in the equation (40) is not diagonal but it reduces to the diagonal matrix $\bar{K}_+$ or $\bar{K}_-$ when the waveguide width is infinite.

On the other hand, the solution of the partial differential equation (1) can be obtained analytically in free space as $e^{i[(k_x+G_p)x\pm k_pz_n]}(p = 0, \pm1, \pm2, ...)$, which corresponds to the p-th element of the field vector $\mathbf{\Phi}_{\pm}(z_n)$. Superposing these solutions with coefficients φ_p and transforming into the field vector, one can obtain the following expression

$$\mathbf{\Phi}_{\pm}(z_n) = \left[e^{\pm ihk_pn}\delta_{p,q}\right]\mathbf{\Phi}_{0\pm}, \tag{53}$$

where $\mathbf{\Phi}_{0\pm}$ is given as $\mathbf{\Phi}_{0\pm} = \{\varphi_p e^{\pm ik_pz_0}\}$. Because the discrete variable solution (50) and the continuous variable solution (53) represent the same plane wave, the relation $e^{\pm ih_zk_p} \approx e_p^{(\pm)}$, must be satisfied with high accuracy. Taking the logarithm of the both sides and expanding the right hand side in power series of h_z, one can obtain the following expression,

$$k_p \approx k_p\Big[1 + \frac{6\theta^2-5}{120}(k_ph_z)^2 - \frac{12\theta^4-20\theta^2+15}{3200}(k_ph_z)^4 + \cdots\Big]. \tag{54}$$

The appropriate value of θ is determined so as to vanish the second term in the right hand side, which is

$$\theta = \sqrt{5/6}. \tag{55}$$

Consequently, the values of α and β are $\alpha = 1/12$ and $\beta = 5/12$, respectively. In this case, the dominat error is detrmined by the last term in the righ hand side of (54) that has the order h_z^4 in magnitude. The fact that the magnitude of the discretization error does not exceed the order of h_z^4 corresponds to Numerov's method that was used to achieve an accurate discretization for the scattering equation [1].

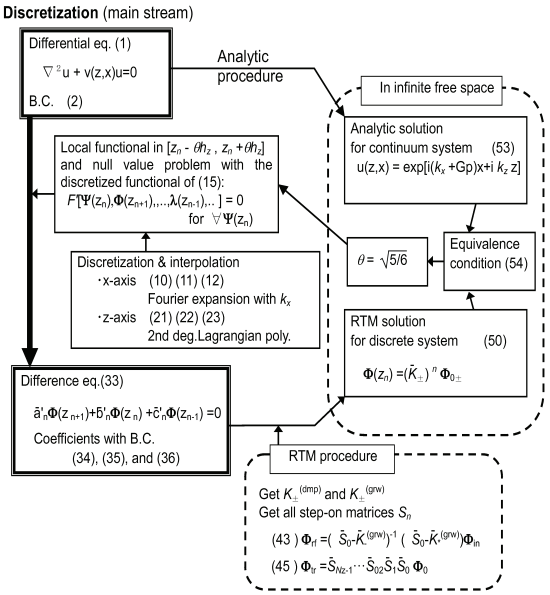

Fig. 2 Scheme to derive the difference equation from the differential equation using the null value problem of F' based on the weak form theory framework.

With the determination of the parameter θ, our aim to construct a novel discretization scheme has been acheved. In Fig. 2 the discretization scheme to derive a difference equation from a differential equation is summarized as a block diagram. The main stream of discretization is realized through the null value problem of the local functional F', (5), which leads to the difference equation (33) according to the weak form theory framework. Moreover, this stream is supported by the discretization and interpolation of the field variables. The sub-stream is the determination of θ that is accomplished through comparison of the continuous and discrete solutions in infinite free space. The RTM procedure is also important to obtain a solution of the discrete system.

3.4 Definition of transmission and reflection rates

The energy flux along the z-axis, J_z, can be defined by the z-component of the Poynting vector expressed as follows,

$$J_z = \frac{1}{2\omega\mu_0}\int_{-a/2}^{a/2}\mathrm{Im}\left[u\frac{\partial u^*}{\partial z}\right]\frac{dx}{a}. \tag{56}$$

For the incident wave, the field $u(z,x)$ can be expressed as $u(z_n,x) = \mathbf{d}(x)(\bar{K}_+^{(\mathrm{grw})})^n\mathbf{\Phi}_{\rm in}$ in the region $z < z_1$. In the definition (56), replacing the partial differential with respect to z with the first-order difference with respect to n leads to the expression of the energy flux for the incident wave, $J_{\rm in}$, as follows,

$$J_{\rm in} = \mathrm{Im}\left[\frac{1}{2\omega\mu_0h_z}\mathbf{\Phi}_{\rm in}^\dagger(\bar{K}_+^{(\mathrm{grw})} - \bar{I})\mathbf{\Phi}_{\rm in}\right], \tag{57}$$

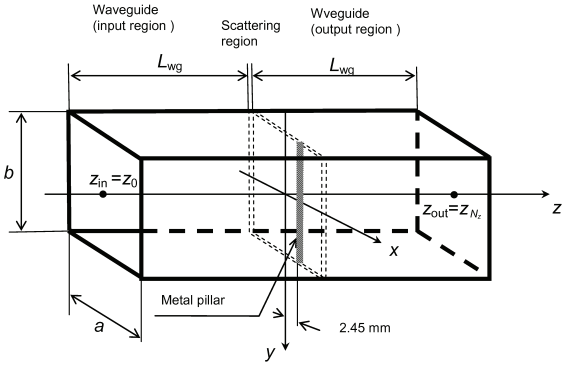

Fig. 3 System composed of a waveguide and metal pillar.

where the notation † is defined by $\mathbf{\Phi}_{\rm tr}^{\dagger} = (\mathbf{\Phi}_{\rm tr}^{*})^{T}$. Applying the same procedure to the energy flux of the reflected wave, $J_{\rm rf}$, and the transmitted wave, $J_{\rm tr}$, yields the following expressions,

$$J_{\rm rf} = {\rm Im}\left[\frac{1}{2\omega\mu_0 h_z}\mathbf{\Phi}_{\rm rf}^{\dagger}(\bar{K}_{-}^{(\rm grw)} - \bar{I})\mathbf{\Phi}_{\rm rf}\right], \tag{58}$$

$$J_{\rm tr} = {\rm Im}\left[\frac{1}{2\omega\mu_0 h_z}\mathbf{\Phi}_{\rm tr}^{\dagger}(\bar{K}_{+}^{(\rm dmp)} - \bar{I})\mathbf{\Phi}_{\rm tr}\right]. \tag{59}$$

Using the definitions of the energy flux, the reflection rate R and transmission rate T can be defined as follows,

$$R = J_{\rm rf}/J_{\rm in}, \quad T = J_{\rm tr}/J_{\rm in}. \tag{60}$$

4. Scattering by a metal pillar asymmetrically placed in the waveguide

4.1 Separation of traveling and localized waves

A significant feature of RTM is that it can extract localized waves around the scatterer. In this section, a scattering phenomenon induced by a metal pillar is used to demonstrate this feature.

In Fig. 3, a schematic configuration of the system is shown. The cross section of the waveguide in the *xy*-plane is rectangular with dimensions a = 15.8 mm and b = 7.6 mm. The waveguides length $L_{\rm wg}$ is 20 mm. The metal pillar has a square cross-section 0.5 mm × 0.5 mm in *zx*-plane and is set parallel to the *y*-axis. The scattering region between the planes denoted by dashed lines has a very thin width that is equivalent to the meal dimension of 0.5mm. The location of the center of the pillar section is x = 2.45 mm and z = 0.25 mm. The material of the pillar was assumed to be stainless steel with a conductance of $\sigma_m = 1.39 \times 10^6 ({\rm cm}\Omega)^{-1}$. The function $v(z, x)$ in (1) can be expressed as follows [5],

$$v(z,x) = \begin{cases} \omega^2\mu_0\epsilon_0 & ,(z,x) \notin \text{pillar} \\ i\omega\sigma_m/\omega & ,(z,x) \in \text{pillar} \end{cases}, \tag{61}$$

where ω is the angular frequency of the microwave, ϵ_0 and μ_0 are the dielectric constant and permeability constant of vacuum, respectively. To be precise, another term exists because of the dielectric constant of the metal; however, the value is negligible for the microwave frequency range under consideration. The discretization steps along the z- and x-axes are chosen as h_z= 0.067 mm and h_x = 0.079 mm, respectively. The step sizes are selected much smaller than the pillar size of 0.5 mm and are also much smaller than the minimum wave length of 15.2 mm being used in the experiment.

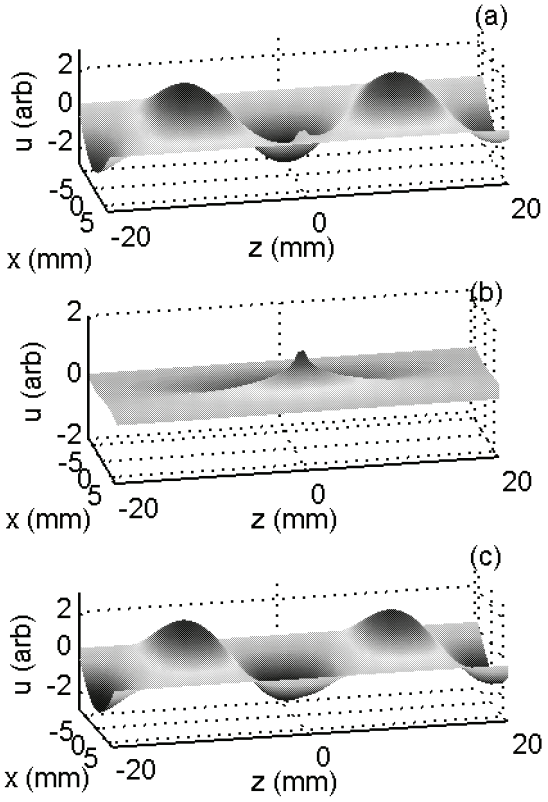

Fig. 4 Surface plots of the electric field around the metal pillar irradiated by the TE_{10} mode wave. (a) Superposition of input and scattering waves, (b) localized wave around the scatterer, and (c) traveling wave including incident, reflected and transmitted waves.

The incident wave is propagating at $z = z_{\rm in}$ and traveling in the positive direction along the z-axis. Assuming the TE_{10} mode, the input field $u_{\rm in}(z, x)$ is given by

$$u_{\rm in}(z,x) = 2\cos(\frac{\pi x}{a})e^{ik_0(z-z_0)}, \tag{62}$$

where κ_0 is the wave number along the z-axis defined as follows,

$$\kappa_0 = \sqrt{\omega^2\mu_0\epsilon_0 - (\pi/a)^2}. \tag{63}$$

Because the parameter k_x is selected as $k_x = \pi/a$ to realize an accurate expansion [4], the field vector $\mathbf{\Phi}_{\rm in}$ of the incident wave is given by

$$\mathbf{\Phi}_{\text{in}} = \{\delta_{p,0} + \delta_{p,-1}\}. \quad (64)$$

In Fig. 4 the surface plots of the electric field around the metal pillar placed in the zx-plane are shown. The incident TE_{10} wave has frequency of 16 GHz. Fig. 4 (a) shows the surface of the electric field that is the superposition of the incident, reflected, transmitted and localized waves. Because of the boundary condition (2), the fields vanish on the surface of the inner walls at $x = \pm a/2$. The surface also avoids the metal pillar because a metal has tendency to reject the electric fields. Though the field distribution outside the metal pillar was obtained with a sufficient accuracy, if the details of the field in the metal pillar are needed, this can be obtained through setting the discretization steps smaller than the skin depth [5].

The localized wave generated around the scatterer or metal pillar is obtained by superposing the modes of the wave constant $\text{Re}[\eta_p] \neq 0$. The surface plot of the extracted localized wave is in Fig. 4 (b) shows the field strength reaches a peak around the metal pillar and decreases away from the pillar. When the scatterer is composed of a layered material, a possible localized wave is the evanescent wave [24] that is generated at the interface of the different materials and an exponentially damping wave tail propagates to the bulk region of the material.

The mode satisfying the condition $\text{Re}[\eta_p] = 0$ corresponds to the traveling wave, *i.e.*, either the incident, reflected or transmitted waves. Fig. 4 (c) shows the extracted traveling waves that are superposition of those waves where the resulting surface is not drained by the metal pillar and is characterized by smooth changes. The superposition of the waves in Figs. 4 (b) and (c) results in the wave shown in figure (a).

The damping tail of the localized waves might reduce the accuracy of the simulation. As an example, the influence of the localized waves in the FEM analysis is described in Appendix B.

4.2 Comparison of experimental and theoretical results

A stainless pillar, as shown in Fig. 3, was fabricated and placed between a pair of coaxial waveguide converters (Agilent P281C). According to the supplier, the standing wave ratio of the converter is less than 1.06. The coaxial lines were connected to a two-port network analyzer (HP 8510). The S-parameter was measured from 9.6 to 18.5 GHz and the influence of the coaxial waveguide converters was eliminated by applying the TRL method [23]. Using the measured S-parameters, the transmission rate T and reflection rate R were obtained from the relations $T = |S_{21}|^2$ and $R = |S_{11}|^2$.

Fig. 5 shows the comparison of the experimental and theoretical data as a function of the incident wave frequency f. In Fig. 5(b), the detail of discrepancy between the experimental and theoretical data is plotted as the ratios T/T_{exp} and R/R_{exp},within the practical frequency range 10 ≤ GHz $f \leq$ 18GHz, where the circles and triangles show ratios of

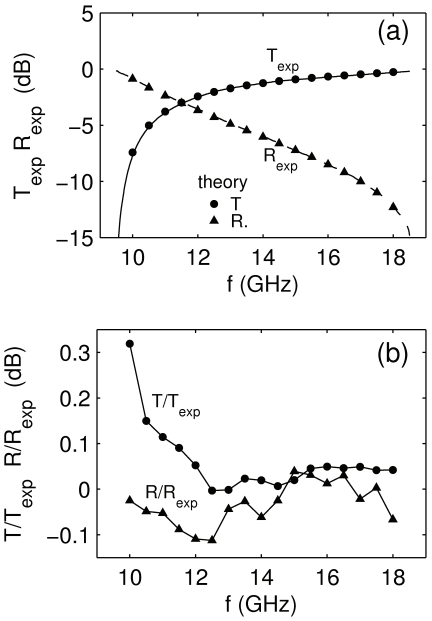

Fig. 5 Comparison of experimental and theoretical values. (a) Frequency dependence of transmission rate T_{exp}, and reflection rate R_{exp}. The theoretical data obtained by RTM are also superimposed with circles for transmission rate T and triangles for reflection rate R. (b) The ratio of theoretical and experimental data of transmission and reflection rates.

respectively, As the frequency f approaches the cut-off frequency of the waveguide, 9.6 GHz, the ratio T/T_{exp} tends to increase, reaching 0.319 dB at f = 10 GHz, but the absolute value of the transmittance is very small, −7.42 dB, as shown in Fig. 5 (a). On the other hand, the upper bound of uncertainties caused by the standing wave ratio is estimated as 0.506 dB. The accuracy of the RTM theory approaches the upper bound being imposed by the standing wave ratio.

5. Conclusion

Using the framework of the weak form theory, a new formulation that utilizes RTM was proposed and applied to microwave scattering in a waveguide. The boundary condition at the inner wall of the waveguide is considered with Lagrangian multipliers which modify the coefficients of the difference equation. The proposed scheme is applicable not only to microwave scattering but also to every phenomenon that can be formulated in the weak form theory framework. To demonstrate the validity of the proposed scheme, we are also planning to analyze flexural waves on an elastic plate.

The proposed theory was applied to a scattering experiment of a metal pillar asymmetrically placed in a waveguide. Discrepancies between the experimental and theoretical values of the transmission and reflection rates were less than the upper bound imposed by the standing wave ratio of the waveguide, which validates our method for practical applications.

As a significant feature of the proposed RTM, the

extraction of the localized wave around the scatterer was demonstrated. This feature can be used to analyze the absorption mechanism of materials with complex shapes.

References

[1] F. Y. Haji, H. Kobeisse and N. R. Nassif, "On the numerical solution of shroedinger's radial equation", Journal of Computational Physics, vol.16, pp.150-159, 1974.
[2] J. A. Appelbaum and D. R. Hamann, "Self-consistent electronic structure of solid surfaces", Physical Review B, vol.6, pp.2166-2177, 1972.
[3] K. Hirose and M. Tsukada, "First-principles calculation of the electronic structure for a bielectrode junction system under strong field and current", Physical Review B vol.51, no.8, pp.5278-5290, Feb. 1995.
[4] H. Kato, M. Kitani and H. Kato, "Recursive transfer method as an accurate numerical method to analyze the scattering of the electromagnetic wave", Trans. IEICE C vol.J94-C, pp.1-9, 2011.
[5] H. Kato and Y. Kanno, "Microwave absorption of catalyst in a thermal decomposition reaction by recursive transfer method", Japanese Journal of Applied Physics, vol.47, no.6, pp.4846-4850, 2008.
[6] P. Solín , Partial differential equations and the finite element method, John wiley & sons, Hoboken 2006.
[7] J. Jin,and D. J. Riley, Finite element analysis of antennas and arrays, John wiley & sons, Hoboken 2009.
[8] KV. A. Klymko, A. B. Yakovlev, I. A., Eshrah, A. A. Kishk, and A. W. Glissoni, "Dyadic Green's function of an ideal and surface circular waveguide with application to excitation and scattering problems", Radio Science, vol.40,doi:10.1029/2004RS003167, 2005.
[9] D. Smith, "Recent advances in regularization techniques for scattering and diffraction", Radio Science, vol.42, doi:10.1029/2007RS003703, 2007.
[10] D. Sjöberg, "Nonlinear waveguides", Radio Science, vol.38, doi:10.1029/2001RS002579, 2003.
[11] F. Mira, A. A.San Blas, V, E. Boria and B. Gimeno, "Wideband impedance matrix representation of passive waveguide components based on cascaded planar junctions", Radio Science, vol.44, RS1004, doi:10.1029/2008RS003886, 2009.
[12] M. Kobayashi, Trans. IECIE C-II, vol.J82-C-II, pp.599-608, 1999.
[13] R. B. Hwang and S. T. Peng, "Scattering and guiding characteristics of waveguides with two-dimensionally periodic walls of finite thickness", Radio Science, vol.38, 1091, doi:10.1029/2002RS002847, 2003.
[14] G. Sztefka and H. P. Nolting, "Bidirectional eigenmode propagation for large refractive index steps", IEEE Photonics Technology Letters, vol.5, pp.554-557, 1993.
[15] M. D. Feit andJ . A. Fleck, "Light propagation in graded-index optical fibers", Applied optics, vol. 17, no. 34, pp. 3990-3998, Dec. 1978.
[16] T, Miyamoto, M. Momoda and K. Yasumoto, "Numerical analysis for 3-dimensional optical waveguides with periodic structure using Fourier series expansion method", Trans. IEICE C, vol.J86-C, pp.591-600, 2003.
[17] Ph. Lambin and J. P. Vigneron, "Improved continued fraction treatment of the one-dimensional scattering problem", Journal of Physics A (Math. Gen.), vol.14, pp.1815-1819, 1981.
[18] S. Ramo, J. R. Whinney, and T. van Duzer, Fields and waves in communication electronics, 3rd ed. John Wiley, New York, 1994.
[19] B. Stout, "Transfer matrix approach to local field calculations in multiple-scattering problems", Journal of modern optics, vol. 49, no. 13, pp. 2129-2152, 2002.
[20] Per Heintz and Klas Samuelsson, "On adaptive strategies and error control in fracture mechanics", Computers and Structures, pp. 485-497 vol. 82, Iss. 6, 2004.
[21] M. J. Forray, Variational calculus in science and engineering, McGraw Hill, New York, 1968.
[22] K. Rektorys, Variational methods in mathematics, science and engineering, D. Reidel Pub., Dordrecht, 1975.
[23] G. F. Engen and C. A. Hoder, "Thru-Reflection-Line: An improved technique for calibrating the dual six-port automatic network analyzer", IEEE Transactions Microwave Theory and Technology, vol. MTT-27, no. 12, pp.987-993, Dec. 1979.
[24] S. Ramo, J. R. Whinnery and T. van Duzer, Fields and waves in comunication electronics (third edition), Jhon Wiley & Sons, New York, 1993.

Appendix A: RTM accuracy on h_z, h_x, and k_x

In Fig. A· 1, the ratio of the theoretical value T and experimental value T_{exp} is shown as a function of the discretization steps h_z and h_x. A typical frequency is of 16 GHz was chosen from a range where the experiment achieves a stable accuracy. The dependence of T/T_{exp} on h_z is very weak, which reflects the fact that the z-axis discretization error of the scattering equation does not exceed the order of magnitude h_z^4, as discussed in section 3.3. The oscillatory behavior of T/T_{exp} with respect to h_x is because of the fact that the field was expanded in a series similar to the Fourier expansion. The black circle in the figure denotes the value used to obtain Fig. 5 (a) and (b), which are h_z = 0.067 mm, h_x = 0.079 mm and T/T_{exp} = 0.0562 dB.

The discretization of the field variables along the x-axis is performed using the Fourier series with an arbitrary parameter k_x as (10) and (11). The Fourier series also plays a role to interpolate the discretized field when obtaining the integrated expression of the functional (15). If the traveling waves (incident, reflected, and transmitted waves) take the TE_{10} mode, selecting $k_x = \pi/a$ has an advantage because the wave can be expressed strictly with the form (64). However, a question arises as to how the accuracy of the RTM depends on the parameter k_x. Below, to try and answer this question, we explore the k_x dependence of T and R.

The p-th component, $\varphi_p^{(\mathrm{in})}$, of the field vector $\mathbf{\Phi}_{\mathrm{in}}$ for cases in which $k_x \neq \pi/a$ is expressed as follows,

$$\varphi_p^{(\mathrm{in})} = \frac{1}{N_x}\sum_{\ell=0}^{N_x-1} 2\cos(\frac{\pi x_\ell}{a})e^{-i(k_x+G_p)x_\ell}. \qquad (\mathrm{A}\cdot 1)$$

Fig. A· 2 shows the k_x dependence of T and $T+R-1$ for an incident wave that vibrates with a frequency of f=16GHz.

Because the expression (A· 1) is periodic with respect to k_x with a period of $2\pi/a$, the rates T and R are also periodic. Fig. A· 2 shows the dependence of just one cycle. Two cases with different step sizes are shown: The small step h_z = 0.067mm, h_x = 0.079mm (solid curves) and the large step h_z = 0.034 mm, h_x = 0.035 mm (dashed curves). The transmission rate T is depicted in a dB scale showing the experimental data T_{exp} (= -0.7128 dB). The reflection rate R versus the experiment data R_{exp} (= -8.5488 dB) is so small that it does not exceed 0.02 dB and is out of range of the vertical scale of Fig. A· 2 (a).

When the scattering system has no energy dissipation, the value of $T + R - 1$ practically vanishes in experiments.

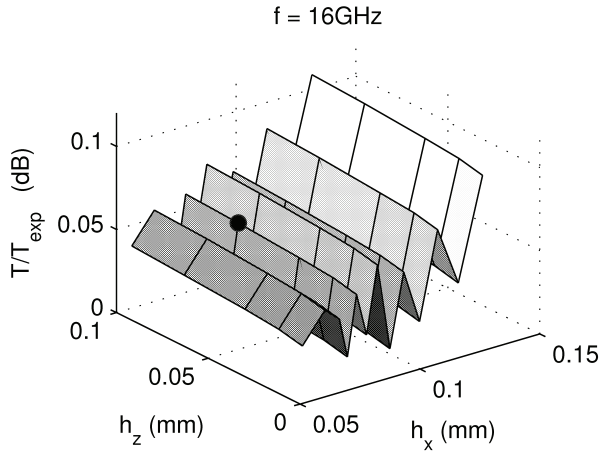

Fig. A·1 Variation of the ratio of the theoretically obtained transmission rate T to the experimentally obtained transmission rate T_{exp} against to the discretization steps h_z and h_x.

Because the metal pillar is very small, the energy dissipation is negligible, this is also confirmed by our experiment where $|T + R - 1| < 0.01$. Therefore, the discrepancy of $T + R - 1$ from the null can be used as an estimator of the analysis error.

The value of $T + R - 1$ has a tendency to increase when $k_x \leq 0$. More specifically, tor the rough mesh case of h_z = 0.034 mm and h_x = 0.035 mm, the discrepancy of the value for $k_x = 0$ is almost eight times that for $k_x = \pi/a$. This discrepancy is because of the expansion error included in (A·1) for $k_x = 0$. The asymmetry of the metal pillar position also causes the asymmetric curves in Fig. A·2 (b). Although Fig. A·2 (b) indicates that the accuracy in both cases is sufficient, the selection of $k_x = \pi/a$ may ensure higher accuracy than that of $k_x = 0$.

Appendix B: Comparison of the RTM and FEM analyses

Using the FEM as an example, we note that the localized wave generated around the scatterer may reduce the accuracy of the transmission and reflection rates.

Using a FEM environment, the scattering problem of the system shown in Fig, 2 is formulated as a two-dimensional TE wave problem where the field variable $u(z, x)$ is the electric field along the y-axis. When an incident wave of the TE_{10} mode comes from the input terminal $z = z_{in}$, the boundary condition at the terminal is expressed by a Newton-Robin type boundary condition as follows,

$$\frac{\partial u}{\partial z} + i\kappa_0 u = i2\kappa_0 X_{10}, \tag{A·2}$$

where κ_0 is the wave number of the TE_{10} mode defined by (63). The function $X_{10}(x)$ is the TE_{10} mode function that can be expressed as $X_{10}(x) = u_{in}(z_0, x)$ with the incident wave $u_{in}(z_0, x)$ defined by (62). At the output terminal $z = z_{out}$, the boundary condition is expressed as a Neuman-type

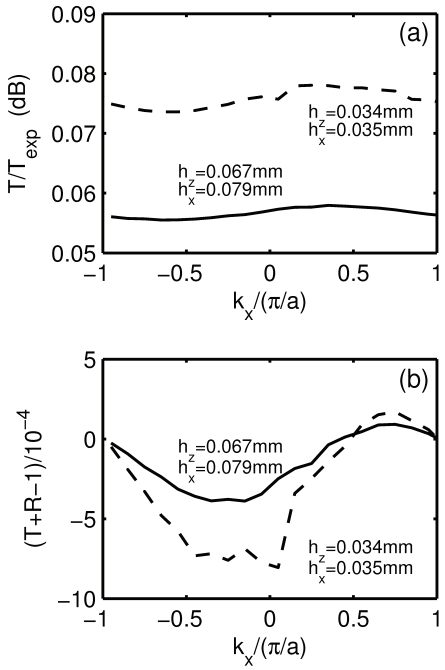

Fig. A·2 k_x dependence of (a) the transmission rate T and (b) the discrepancy of $T + R - 1$ from the null value. Solid and dashed curves show the small and large didcretization steps, respectively.

boundary condition as follows,

$$\frac{\partial u}{\partial z} = i\kappa_0 u. \tag{A·3}$$

The fields are also assumed to vanish at the inner walls of the waveguide and at the surface of the metal pillar considering the metal is a perfect conductor.

Using numerical wave forms at the input terminal, $X_{in}(x) = u(z_{in}, x)$, and at the output terminal, $X_{out}(x) = u(z_{out}, x)$, one can define the transmission rate T and the reflection rate R as follows,

$$T = \left| \frac{\int_{-a/2}^{a/2} X_{10}^*(X_{in} - X_{10})dx}{\int_{-a/2}^{a/2} X_{10}^* X_{10} dx} \right|^2, \tag{A·4}$$

$$R = \left| \frac{\int_{-a/2}^{a/2} X_{10}^* X_{out} dx}{\int_{-a/2}^{a/2} X_{10}^* X_{10} dx} \right|^2. \tag{A·5}$$

Because the mode function $X_{10}(x)$ is not orthogonal to the localized waves, the values of T and R are affected by the amount of the localized wave included in the functions $X_{in}(x)$ and $X_{out}(x)$. To exclude the localized wave, one has to choose the waveguide length L_{wg} so that it is longer than the tails of the localized wave.

Fig. A·3 shows the frequency dependence of T and R for various waveguide lengths L_{wg}. The FEM environment and parameters used for the calculation are as follows: the interpolation function is the second-order Lagrange polynomial, the total numbers of mesh triangles 424, 415, and 133

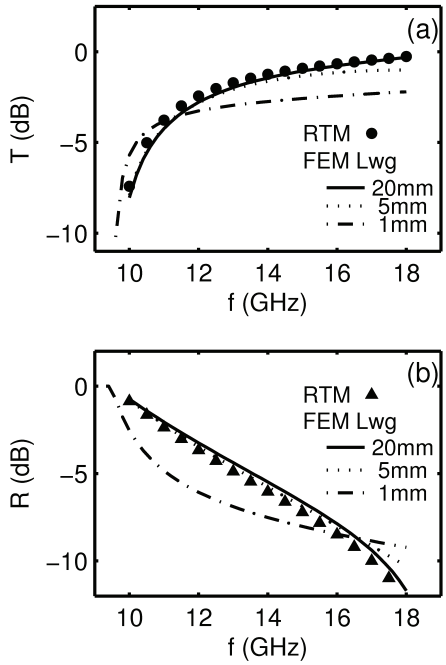

Fig. A·3 Frequency dependence of (a) the transmission rate T and (b) the reflection rate R for various waveguide lengths. The solid, dotted, and the dot-dashed curves represent L_{wg} = 20 mm, 5 mm, and 1 mm, respectively, and the black circles and triangles show the data obtained by RTM.

for L_{wg} = 20 mm, 5 mm, and 1 mm, respectively. The RTM data are equivalent to those in Fig. 5 and do not depend strongly on the length L_{wg}. Though the results of FEM and RTM agree quite well for L_{wg} = 20 mm, the discrepancies of both T and R increase as L_{wg} decreases, more specifically, for the case of L_{wg} = 1 mm, where the deterioration of the FEM analysis is crucial. On the other hand, RTM agrees with the experimental data shown in Fig. 5 even if the length L_{wg} is very short provided that the length L_{wg} is at least two times larger than the step size h_z.